A NUMERICAL STUDY ON THE SUPPRESSION OF A DETRIMENTAL WELD POOL PROFILE IN WIRE FEED LASER BEAM WELDING BY MAGNETOHYDRODYNAMIC TECHNIQUE

X. MENG*, A. ARTINOV*, M. BACHMANN*, Ö. ÜSTÜNDAĞ*, A. GUMENYUK*, M. RETHMEIER**,***,*

**BAM Bundesanstalt für Materialforschung und -prüfung, 12205, Unter den Eichen 87, Berlin, Germany*
***Technical University Berlin, Institute of Machine Tools and Factory Management, 10587, Pascalstraße 8-9, Berlin, Germany*
****Fraunhofer Institute for Production Systems and Design Technology, 10587 Pascalstraße 8-9, Berlin, Germany*

DOI 10.3217/978-3-85125-968-1-08

ABSTRACT

The weld quality and the possible defect formation are directly determined by the weld pool shape and the thermo-fluid dynamics therein. In this paper, an untypical weld pool profile, i.e., elongated at its top and bottom but narrowed at the middle, is found experimentally and numerically in the wire feed laser beam welding. The detrimental influence of the weld pool narrowing on the element transport is analyzed and discussed. A magnetohydrodynamic technique is utilized to suppress the narrowing, aiming at a more homogenous element distribution. It is found that a low-temperature region is formed in the middle of the weld pool due to the interaction of the two dominant circulations from the top and bottom regions. The weld pool is significantly narrowed due to the untypical growth of the mushy zone in the low-temperature region, which results in a direct blocking effect on the downward flow and the premature solidification in the middle region. The Lorentz force produced by a transverse oscillating magnetic field shows the potential to change the flow pattern into a single-circulation type and the low-temperature-gradient region is mitigated. Therefore, the downward transfer channel is widened, and its premature solidification is prevented. The numerical results are well validated by experimental measurements of metal/glass observation and X-ray fluorescence element mapping.

Keywords: thermo-fluid flow, element transport, laser beam welding, magnetohydrodynamics, multi-physical modeling

INTRODUCTION

Laser beam welding (LBW) has attracted more and more academic and industrial attention during the last decades. It shows several superiorities, e.g., precise and highly localized heat input, excellent penetration capacity, low distortion, *etc*. Nonetheless, the utilization of the small laser spot and the resulting high energy density may lead to drawbacks during the practical application of the LBW process. The small laser spot

makes the weld seam sensitive to assembly tolerances of the workpieces. Furthermore, a non-negligible loss of important alloying elements, e.g., Mg or Zn in Al alloy, may occur due to vigorous evaporation [1].

The issues described above can be mitigated or solved by the usage of filler wire, namely, the wire feed laser beam welding (WFLBW). The gap tolerance sensitivity can be significantly reduced by the liquid filler metal. By choosing a filler wire with proper chemical composition, important alloying elements can be supplemented to the weld pool, thus achieving better control over the metallurgical process. However, the weld pool with narrow and deep geometry and high solidification rate causes difficulties in the downward transfer of the filler metal. Often, the filler material accumulates on the upper part of the final weld, undermining the homogeneity of the weld properties [2].

It has been confirmed in numerous studies that during partial penetration LBW the weld pool is typically elongated at the upper region, driven by the recoil pressure and the Marangoni shear stress, compared to the relatively short bottom region [3-6]. Recently, a different type of weld pool shape was observed both experimentally and numerically [7-9]. The weld pool boundary is elongated at the top region and bottom region but significantly narrowed in the middle. Up to now, only a few works have been reported on this untypical weld pool narrowing and its influence on the transport phenomena. It can be easily foreseen that the narrowed region may further deteriorate the downward transport of the filler metal once it is formed during the WFLBW.

Since 2000, magnetohydrodynamic (MHD) technology has shown more and more importance to improve the capacity of the traditional LBW. Different beneficial effects can be produced by choosing a magnetic field with proper position, strength, frequency, and orientation, such as deceleration of the liquid metal in the weld pool [10], electromagnetic support against gravity to eliminate sagging of the weld seam [11], electromagnetic exclusive force to suppress porosity [12], and refinement of the grain structure [13]. The work of Gatzen suggested that during WFLBW of Al alloys, the Si from the filler wire was mixed more uniformly when employing a coaxial alternating magnetic field with a frequency below 25 Hz [14]. In the authors' previous study, a transverse high-frequency magnetic field was imposed from the top side of the workpiece during WFLBW of austenitic steel with filler wire of nickel-based Inconel 625 alloy [15].

As the computational capacity improves, the multi-physical modeling provides great potential to obtain quantitative descriptions of the weld pool behavior under the influence of a magnetic field. A three-dimensional steady-state MHD model with a predefined keyhole profile was developed by Bachmann et al [16-18]. The influences of static and alternating magnetic fields on the weld pool behavior and its prevention of the sagging defect were investigated. The onset of the bulging phenomenon which was characterized by an elongation of the bottom region was reported in the study as well but the impact of the magnetic field on this phenomenon was not further discussed [18]. The enhancement of the material mixing in the weld pool from a low-frequency coaxial magnetic field was explained by Gatzen et al. using an MHD model with a fixed keyhole [19]. The inhomogeneity problem of the element distribution was moderated, but a spatial periodicity of the concentration remained due to the periodic Lorentz force.

Recently, more sophisticated MHD models were developed, in which the free surface tracking algorithm such as volume-of-fluid (VOF) or level-set method was implemented to calculate the transient keyhole shape [20, 21]. Different beneficial effects from the

LBW with a magnetic field, including sagging defect elimination by the electromagnetic support and grain refinement by the thermoelectric current effect, were investigated more deeply. A multi-physical model with the transient keyhole evolution was developed by the authors for the investigation of the electromagnetic stirring enhanced wire feed laser beam welding (EMS-WFLBW) [22-24]. It should be noted that the weld pool in the above studies shows a common shape, i.e., elongated at the upper region and relatively short at the bottom. The problem of inhomogeneous element distribution originates from the steep weld pool shape and the high solidification rate which are inevitable during all deep-penetration LBW processes.

In the present study, a narrowing phenomenon in the middle of the weld pool during WFLBW is found by a real-time metal/glass observation and a multi-physical modeling. An X-ray fluorescence (XRF) element mapping is implemented for the characterization of the material mixing. The formation mechanism of the weld pool narrowing is analyzed and its resulting detrimental effect on the element transport is discussed. By introducing an external oscillating magnetic field, the narrowed region is successfully suppressed, providing a better material mixing in the final weld seam. The influences of the Lorentz force on the transport phenomena in the weld pool and the suppression of the weld pool narrowing are studied as well.

EXPERIMENTAL SETUP

The base metal was chosen as AISI 304 stainless steel, and the filler wire was NiCr20Mo15 alloy with a diameter of 1.1 mm. A distinct difference in the Ni content existed between the base metal and the filler material (9 % vs. 64 %). The dimensions of the base metal were 200 mm × 60 mm × 10 mm. The laser beam welding was performed with an IPG YLR 20000 laser system. The detailed welding parameters are listed in Table 1.

Table 1 Welding parameters and laser optical parameters

Welding parameters	Value
Laser power	6.5 kW
Welding speed	1.3 m/min
Wire feeding rate	2.1 m/min
Wire feed angle	33°with respect to the base metal
Shielding gas flow rate	20 L/min
Laser spot diameter at the focal plane	0.56 mm
Wavelength	1070 nm
Focal position	- 3.0 mm

An in-house designed electromagnet was employed to produce sufficient magnetic flux density and frequency [12]. The electromagnet was fixed 2 mm above the base metal. A Hall sensor was used to measure the spatial distribution of the magnetic flux density in cold metal conditions. A metal/glass configuration was applied to observe the real-time weld pool profile in the longitudinal section without filler material [25]. A high-speed camera operating at the frame rate of 3000 Hz was used to capture the weld pool shape from the metal/glass interface. The optical axis of the lens was parallel with the welding plane and perpendicular to the welding direction.

After the welding experiment, the metallurgical specimens were mechanically cut from the weld specimens for transverse and longitudinal observation. The specimens were ground, polished, and etched by a V2A etchant (100 ml H_2O, 100 ml HNO_3, and 10 ml HCl). XRF mapping was conducted to measure the Ni content on the longitudinal section to characterize the material mixing.

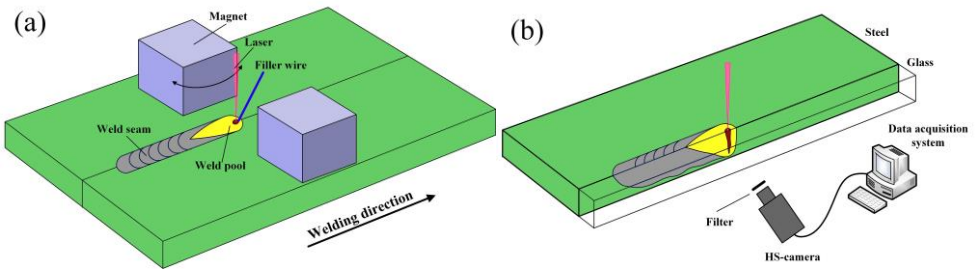

Fig. 1 Schematic of the experimental setup: (a) EMS-WFLBW, (b) metal/glass observation

MATHEMATICAL MODELING

A 3D MHD model coupled with the VOF algorithm and element transport equation is developed to calculate the temperature and velocity fields, the keyhole dynamics, the element transport, and the electromagnetic phenomena in both WFLBW and EMS-WFLBW. The flow regime in the weld pool is considered laminar, and the fluid is assumed as Newtonian and incompressible.

GOVERNING EQUATIONS

The keyhole geometry, as well as the weld pool free surface, is tracked by the VOF method, which is governed by the following equation:

$$\frac{\partial F}{\partial t} + \nabla \cdot \left(\vec{v} F \right) = S_F \tag{1}$$

where F is the volume fraction, t is the time, $\vec{v}$ is the velocity vector and S_F is the source term from the filler metal. The free surface, more precisely the interface between the steel and the Ar gaseous phase, is located within the cells with a volume fraction between 0 and 1.

The transport phenomena can be calculated by solving the conservation equations of mass, momentum, energy, and chemical species, which are defined as follows:

$$\nabla \cdot \vec{v} = \frac{m_w}{\rho} \tag{2}$$

$$\rho\left(\frac{\partial \vec{v}}{\partial t}+\left(\vec{v}\cdot\nabla\right)\vec{v}\right)=-\nabla p+\mu\nabla^2\vec{v}-\mu K\vec{v}+m_{\mathrm{w}}\vec{v}_{\mathrm{w}}+\vec{S}_{\mathrm{m}} \tag{3}$$

$$\rho\left[\frac{\partial h}{\partial t}+\vec{v}\cdot\nabla h\right]=\nabla\cdot\left(k\nabla T\right)+h_{\mathrm{w}}+S_q \tag{4}$$

$$\frac{\partial F_{\mathrm{s}}\rho_{\mathrm{s}}w}{\partial t}+\nabla\cdot\left(F_{\mathrm{s}}\rho_{\mathrm{s}}\vec{v}w-F_{\mathrm{s}}D\nabla w\right)=S_{\mathrm{add}} \tag{5}$$

In Eq. (2), ρ is the density, m_w is the volumetric mass flow rate from the filler wire. In Eq. (3), p is the pressure, μ is the dynamic viscosity, $\vec{v}_w$ is the velocity of the molten filler metal, K is the Carman–Kozeny equation coefficient, which is responsible for the deceleration of the liquid in the mushy zone, and $\vec{S}_{\mathrm{m}}$ is the momentum source term. In Eq. (4), T is the temperature, k is the thermal conductivity, h is the enthalpy, h_w is the energy source from the molten filler metal, and S_q is the additional energy source term. In Eq. (5), w is the weight percentage, F_{s} is the steel volume fraction, D is the diffusion coefficient of Ni-atoms in iron, and S_{add} is the source term from the filler wire.

A magnetic induction equation, rather than the full set of Maxwell equations, is solved for the MHD behavior. This method does not require including the electromagnet in the simulation domain. Instead, the experimentally measured external magnetic field $\vec{B}_0$ is implemented as input data, as given below:

$$\frac{\partial \vec{b}}{\partial t}+\left(\vec{v}\cdot\nabla\right)\vec{b}=\frac{1}{\mu_{\mathrm{m}}\sigma_{\mathrm{e}}}\nabla^2\vec{b}+\left(\left(\vec{B}_0+\vec{b}\right)\cdot\nabla\right)\vec{v}-\left(\vec{v}\cdot\nabla\right)\vec{B}_0 \tag{6}$$

where μ_{m} is the magnetic permeability, σ_{e} is the electrical conductivity, $\vec{b}$ is the induced magnetic field from the liquid flow. For simplification, the solidified 304 stainless steel is assumed to keep a perfectly austenitic microstructure, thus μ_{m} is set to 1.

By using $\vec{B}_0$ and $\vec{b}$, the induced Lorentz force which is the driving force from the MHD technique to adjust the weld pool behavior can be calculated as:

$$\vec{j}=\frac{1}{\mu_m}\nabla\times\left(\vec{B}_0+\vec{b}\right) \tag{7}$$

$$\vec{F}_{\mathrm{L}}=\vec{j}\times\vec{B}=\vec{j}\times\left(\vec{B}_0+\vec{b}\right) \tag{8}$$

where $\vec{j}$ is the current density and $\vec{F}_{\mathrm{L}}$ is the Lorentz force.

PHYSICAL MODELS AND NUMERICAL IMPLEMENTATION

A ray tracing method with a virtual refinement technique is implemented to calculate the multiple reflections of the laser beam and the Fresnel absorption on the keyhole surface. The laser beam was discretized by a sufficient number of sub-rays, and each sub-ray had its location-dependent energy density and initial incidence angle [26]. The laser energy input together with the energy dissipation due to convection, radiation, and evaporation

was employed in the model for the calculation of the temperature field. The recoil pressure as a function of the local temperature [27] was applied to the keyhole surface. The dynamic balance between recoil pressure, hydrostatic pressure, hydrodynamic pressure, and Laplace pressure was calculated to determine the transient keyhole geometry. The thermo-capillary flow driven by the steep temperature gradient on the top surface of the weld pool and the buoyancy based on the Boussinesq approximation were considered as well. Due to the application of the VOF method, all surficial terms should be converted into localized volumetric terms using the continuum surface force method [28]. Therefore, physical mechanisms that contribute to the $\vec{S}_{\mathrm{m}}$ term included recoil vapor pressure, surface tension, and Marangoni stress. The laser heat flux and the thermal dissipation were also converted and implemented in the S_q term.

ANSYS Fluent 19.5 was used to solve all transport equations, in which the second order upwind method was utilized for the spatial discretization of the convection-diffusion equations. The PISO algorithm was applied for the pressure-velocity coupling. A simulation with a physical time of 1.5 s was calculated firstly for the reference case of WFLBW. The obtained data were used as the initial condition for the subsequent calculation of MHD cases (1.5 s - 3.0 s). Table 2 lists the multiple simulation cases with different electromagnetic parameters.

Detailed descriptions of the physical models, boundary conditions, numerical considerations, etc. can be found in the authors' previous studies [22-24].

Table 2 Electromagnetic parameters used in the investigation

Case	Magnetic flux density (mT)	Frequency (kHz)	Angle with respect to transverse direction (deg)	Approach
Ref	-	-	-	Num. & Exp.
1	250	3.6	10	Num. & Exp.
2	250	1.8	10	Num.
3	190	3.6	10	Num.
4	125	3.6	10	Num.

RESULTS AND DISCUSSION

MODEL VALIDATION

A comparison of the fusion line shapes between the experimental and numerical results is provided in Fig. 2. The model shows a high accuracy in predicting the weld penetration as well as the weld width. The energy absorption on the keyhole surface and the energy allocation inside the weld pool are influenced by the Lorentz force by changing the keyhole dynamics and the backward flow of the liquid metal [23].

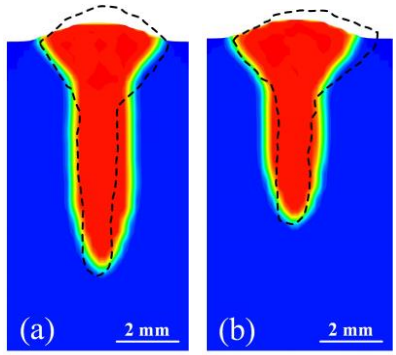

Fig. 2 Fusion line shapes from the calculations and experiments: (a) reference case, (b) case 1

The calculated Ni distributions along the longitudinal section are compared with the XRF mapping in Fig. 3 for further validation of the model. The final weld from the WFLBW shows a quite inhomogeneous Ni distribution, in which the top Ni-rich zone and the bottom Ni-poor zone are sharply separated by a narrow transition region, as shown in Fig. 3 (a) and (b). The downward transport of the filler metal is significantly enhanced under an oscillating magnetic field (250 mT, 3.6 kHz, 10°), resulting in an improved element dilution, as seen in Fig. 3(c) and (d). The proposed model also provides a successful prediction of this phenomenon. Thus, it can be concluded that the established MHD model can provide an accurate prediction of the element distribution.

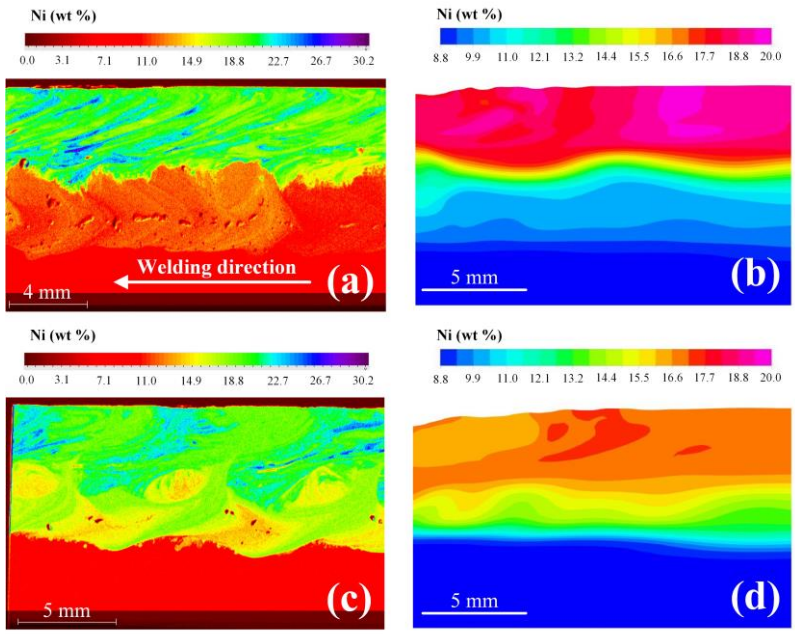

Fig. 3 Calculated and XRF-measured Ni distribution on the longitudinal section: (a) and (b) from reference case, (c) and (d) from case 1

The transient weld pool profile can be obtained by the metal/glass observation, as shown in Fig. 4. It should be noted that it is only a compromised way by far to experimentally validate the existence of the narrowed region in the WFLBW since the filler wire cannot be introduced in the metal/glass setup. In Fig. 4(a), the laser optical axis is located at the interface between the metal and the glass, thus the symmetrical plane of the weld pool is expected to be observed. The keyhole with high-temperature metal vapor shows the highest brightness in the image. Two strong circulations are formed in the top and bottom regions, respectively, and a noticeable narrowed region in the middle of the weld pool can be identified. The calculated liquid metal flow in Fig. 4 (b) shows a similar pattern compared to the experimental image, and the narrowing phenomenon in the middle region is also reproduced by the model. The solid lines correspond to the solidus and liquidus isotherms. The impact of the absence of the filler wire during the metal/glass observation can hardly be evaluated, making the quantitative comparison between Fig. 4 (a) and (b) challenging. Nevertheless, it can still be confirmed qualitatively that the developed multi-physical model has the capacity to reproduce the narrowing phenomenon in the WFLBW.

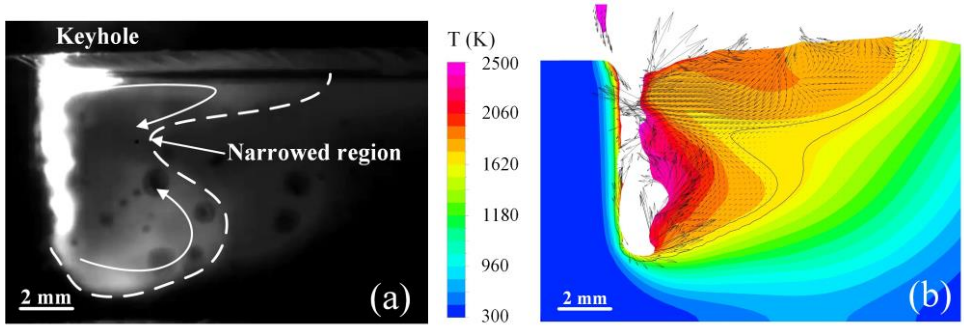

Fig.4 Comparison of weld pool shapes between (a) meta/glass observation and (b) numerical calculation

FORMATION OF THE NARROWING PHENOMENON

As seen in Fig. 4, there are two predominant circulations in the fully developed weld pool. In the upper region, the liquid metal flows backward along the free surface, and then the flow is redirected to flow forward in the longitudinal section. This circulation contributes to the elongated profile of the weld pool and the sufficient material mixing in the upper region. Starting from the bottom of the keyhole, the liquid metal flows backward and upward along with the S/L interface, and subsequently toward the keyhole rear wall, forming the bottom vortex. A confluence of the two circulations is found in the middle region where the untypical narrowing occurs.

According to the available literature, it can be found that either the upper circulation [26, 29] or the lower circulation [30, 31] may dominate the weld pool flow in partial penetration LBW. Both flow patterns will produce a typical weld pool shape, i.e.,

elongated at the top and shortened at the bottom. The flow pattern in Fig. 4(b) which is dominated by two circulations with similar intensities may lead to a unique energy allocation in the weld pool. The free surface of the keyhole receives the laser energy from direct irradiation. For the bulk of liquid metal in the weld pool, the keyhole surface is an equivalent heat source. As the liquid metal flow with higher temperature leaves the vicinity of the keyhole, its enthalpy is gradually transferred into the surrounding liquid metal, which is the dominant energy transfer mechanism from the keyhole to the weld pool. The middle region is where the two circulations end, implying that it receives the least energy from the keyhole.

It should be noted that the liquidus line is significantly narrowed in the middle region, and the solidus boundary, on the contrary, has relatively inapparent narrowing. It results in a mushy zone thickness of up to 3.5 mm between the liquidus and solidus lines. By ignoring the mechanical gouging from the liquid metal, the geometry of the S/L interface is principally determined by the temperature gradient ahead of it [32]. A thermal equilibrium should be built in the S/L region of a weld pool in the quasi-steady state, which means that the energy entering through the liquidus boundary should be equal to the energy leaving the S/L region. The problem can be simplified into a one-dimensional thermal model if the metal flow in the mushy zone is neglected and a linear variation of temperature gradient G along the solidification direction is assumed:

$$k_{\mathrm{l}} G_{\mathrm{l}} \approx k_{\mathrm{mu}} \frac{2\left(T_{\mathrm{L}} - T_{\mathrm{S}}\right)}{\delta_{\mathrm{mu}}} \tag{9}$$

where k_{l} is the thermal conductivity at the liquidus temperature, G_{l} is the temperature gradient at the liquidus line, k_{mu} is the averaged thermal conductivity in the mushy zone, and δ_{mu} is the mushy zone thickness. It should be noted that a factor of 2 is used in Eq. (9) for the correction of using the linear term [33].

Fig. 5 shows the temperature gradient along the longitudinal section. It is found that a low-temperature-gradient region forms at the confluent area of the two circulations where the temperature gradient is only 2×10^4 K/m - 3×10^4 K/m. By substituting the typical values (k_{l} = 33 W/m·K, k_{mu} = 31 W/m·K, $G_{\mathrm{l}} = 2.5 \times 10^4$ K/m) into Eq. (9), the mushy zone thickness is calculated as 4.1 mm, which is close to the numerical value of 3.2 mm. The result from the simplified one-dimensional model shows an acceptable agreement with the numerical outcome, implying that the model captures the main physical feature for the formation of the narrowed region. Therefore, it can be inferred that the formation of the low-temperature-gradient region directly leads to the untypical narrowing in the middle region of the weld pool.

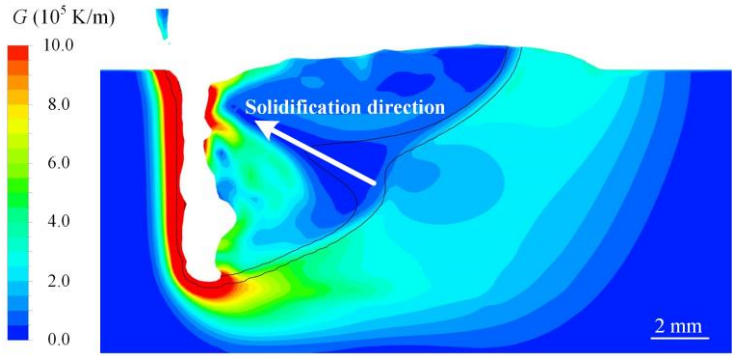

Fig. 5 Temperature gradient in the longitudinal section in reference case

SUPPRESSION OF NARROWING BY MHD TECHNIQUE

The inhomogeneous element distribution has been recognized as a common problem in WFLBW even if the weld pool has no narrowed region [15, 23, 24]. In the present study, the narrowing phenomenon may lead to further deterioration of the material mixing in the weld pool. A time-averaged z velocity component within 0.3 s along the thickness direction (Line AB) in the longitudinal section is plotted in Fig. 6 The liquid metal shows a positive component of the z velocity component in the region near the rear keyhole wall (Line AB). The z velocity component can reach up to +0.05 m/s in the bottom region, but it decreases dramatically to nearly zero after flowing across the narrowed region. From the viewpoint of mass transfer, the weld pool is segmented by the narrowing region, which is apparently detrimental to material mixing.

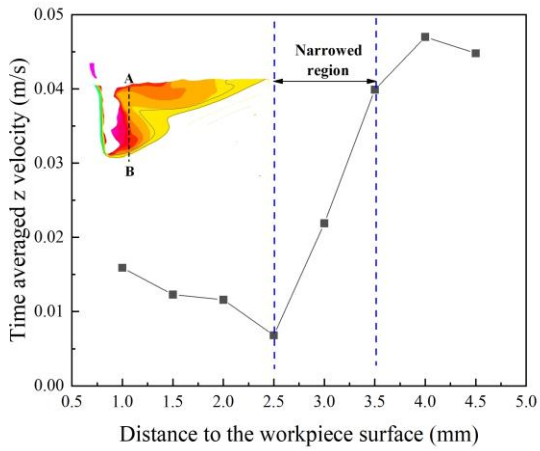

Fig. 6 Time-averaged z velocity along the thickness direction in reference case, in which positive value represents upward velocity

Without the narrowing phenomenon, the weld pool shows a typical solidification sequence, i.e., it starts at the region near the fusion line, and the S/L interface moves toward the region near the central line [34-36]. Hereby, the channel for the downward transfer of the filler material remains open during the whole solidification procedure. A premature solidification occurs in the middle region of the transfer channel when the narrowed region is formed. At the position of 3 mm from the center of the keyhole, the middle region has solidified completely, preventing the downward transport of the filler metal.

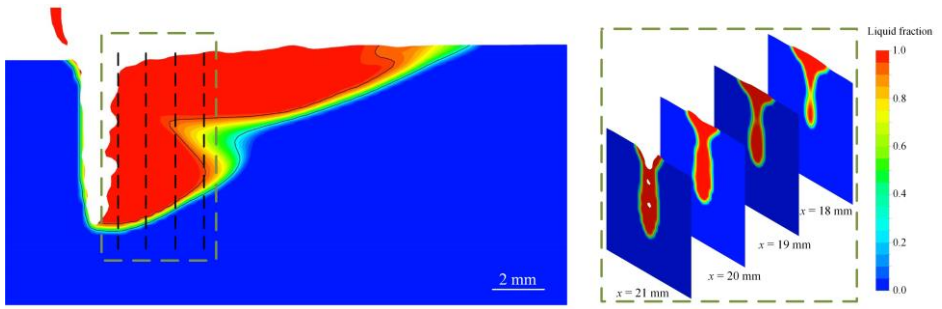

Fig. 6 Premature solidification caused by the narrowing of the weld pool

The influence of magnetic field under a representative set of welding parameters causing the narrowing phenomenon is focused in this paper. The complex relationship between the welding parameters and magnetic parameters is not further discussed. As seen in Fig. 7, the narrowed region in the middle region of the weld pool is almost eliminated by a magnetic field of 250 mT and 3.6 kHz. More specifically, the thick mushy zone is diminished under the induced Lorentz force, from 3.5 mm to 0.7 mm. Previous studies suggest that a transverse oscillating magnetic field applied from the top side of the workpiece produces a time-averaged downward Lorentz force in the weld pool [16]. This Lorentz force produces a downward stream of liquid metal with a velocity of -0.05 m/s along Line AB. This flow pattern has a positive influence on the downward transport of the filler metal, improving the mixing in the final weld.

On the other hand, the Lorentz force also shows a significant influence on the solidification sequence of the weld pool, see Fig. 8. The premature solidification occurring in the reference case is eliminated, thus the downward transfer channel remains open. It provides an additional benefit to material mixing.

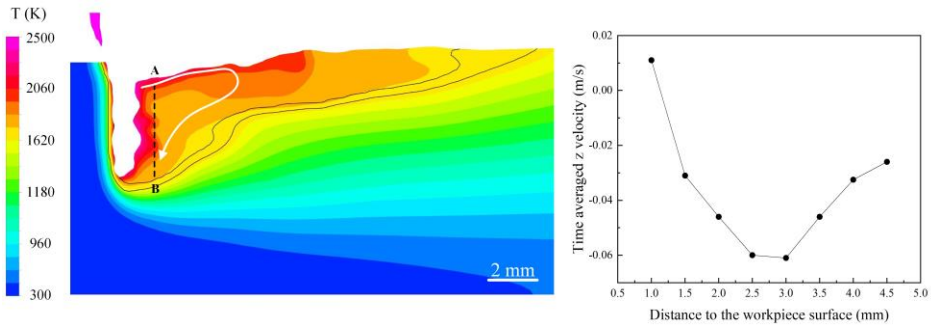

Fig. 7 Weld pool profile (left) and time-averaged z velocity along the thickness direction (right) in case 1

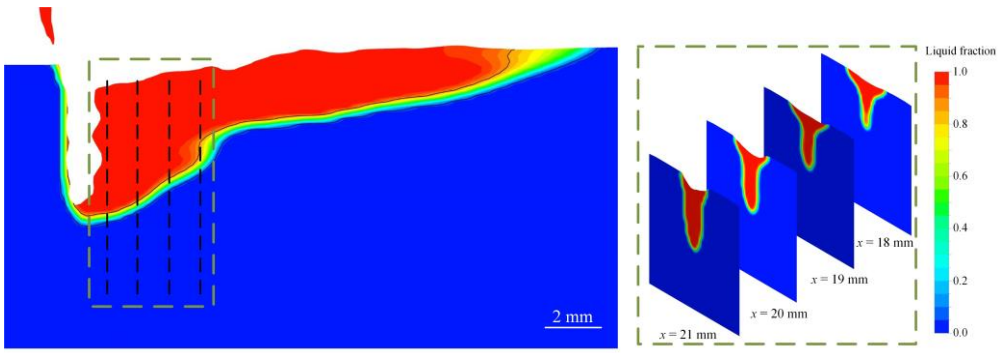

Fig. 8 Solidification sequence of the weld pool in case 1

The Lorentz force contributes to the suppression of the weld pool narrowing from two aspects: by changing the temperature gradient in front of the liquidus boundary and by the direct mechanical gouging effect. Firstly, the flow regime varies from the two-circulation pattern into a single-circulation pattern, as shown in Fig. 7 by the white arrow. More energy can be transferred from the keyhole region to the middle region, which leads to the variation of temperature gradient in front of the liquidus boundary in Fig. 9. By substituting $G_l = 9 \times 10^4$ K/m into Eq. (9), a value of 1.2 mm for δ_{mu} is obtained, which is in the right order of magnitude with the numerical results of 0.7 mm. It indicates that the change of the temperature gradient mainly contributes to the elimination of the narrowing. However, it shows a relatively larger error caused by the neglected mechanical gouging effect. The liquid metal flows vertically to the solidification direction, producing a stronger gouging effect on the S/L interface, which results in a thinner mushy zone.

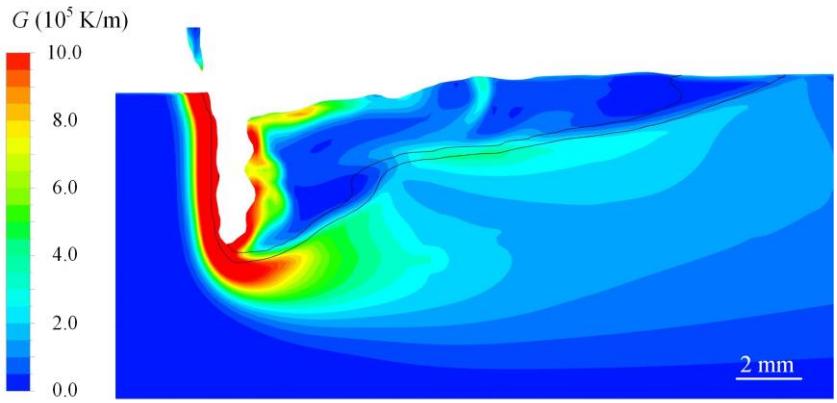

Fig. 9 Temperature gradient in the longitudinal section in case 1

According to the above analysis, the thickness of the mushy zone in the middle region can be considered as an index to describe the extent of the narrowing. By involving the dimension of the weld pool, a dimensionless mushy zone thickness can be written as

$$\delta_{\mathrm{mu}}^{*} = \delta_{\mathrm{mu}} / w_{\mathrm{WP}} \tag{10}$$

where w_{WP} is the width of the weld pool in the middle region. Higher δ_{mu}^{*} means more pronounced weld pool narrowing. Different δ_{mu}^{*} together with the averaged Ni content at the weld bottom under different magnetic flux densities are plotted in Fig. 10. When the magnetic flux density is below 125 mT, the Lorentz force cannot produce apparent suppression on the detrimental narrowing, whereby no improvement of mixing is obtained compared with the reference case. When the magnetic flux density increases from 125 mT to 250 mT, the dimensionless mushy zone thickness decreases dramatically from 0.39 to 0.18. It means that both the direct blocking effect caused by the narrowed region and the premature solidification are inhibited, thus the Ni increment reaches up to 5.7 %.

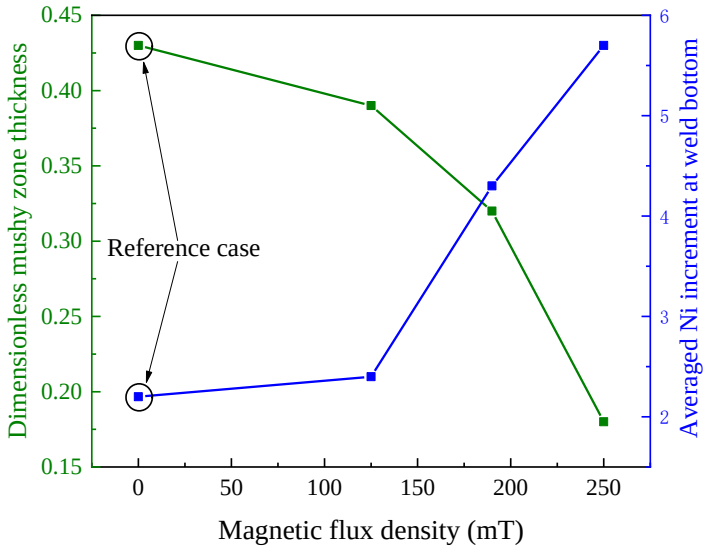

Fig. 10 Influence of the magnetic flux density on the dimensionless mushy zone thickness and the averaged Ni content

CONCLUSIONS

In the present study, multi-physical modeling and experiments are utilized to study an untypical narrowing phenomenon in the weld pool during WFLBW. The detrimental effect of the narrowed region on the material mixing is evaluated. An MHD technique is introduced to suppress the narrowing to achieve better material mixing. The main conclusions are drawn below:

- (1) The narrowing may occur when the weld pool flow is dominated by two circulations at the top and bottom regions. A low-temperature-gradient region forms, which leads to the untypical growth of the mushy zone, and correspondingly, the narrowing of the weld pool.
- (2) The narrowing phenomenon produces a direct blocking effect on the mass transport between the top and bottom regions. Premature solidification of the weld pool in the middle region is also caused by the narrowing, and thereby the downward transfer channel is closed completely.
- (3) The narrowing can be suppressed with a transverse oscillating magnetic field. Under the driving of the Lorentz force, the liquid metal flows downward, thus changing the flow pattern from two-circulation to a single-circulation type. The low-temperature-gradient region is mitigated, which significantly thins the mushy zone. The weld pool will not solidify prematurely in the middle region once the narrowed region is fully suppressed.

ACKNOWLEDGEMENTS

This work is funded by the Deutsche Forschungsgemeinschaft (DFG, German Research Foundation) – project Nr. 416014189 (BA 5555/6-1) and Nr. 411393804 (BA 5555/5-2) .

References

[1] A. DILTHEY, A. GOUMENIOUK, V. LOPOTA, G. TURICHIN, E. VALDAITSEVA: 'Development of a theory for alloying element losses during laser beam welding', *J. Phys. D-Appl. Phys*., 34 (1) (2001), 81.

[2] X. MENG, A. ARTINOV, M. BACHMANN, M. RETHMEIER: 'Numerical study of additional element transport in wire feed laser beam welding', *Procedia CIRP*, 94 (2020), 722-725.

[3] S. KATAYAMA, Y. KAWAHITO, M. MIZUTANI: 'Elucidation of laser welding phenomena and factors affecting weld penetration and welding defects', *Phys. Procedia*, (2010) 5, 9-17.

[4] Y. KAWAHITO, Y.UEMURA, Y. DOI, M. MIZUTANI, K. NISHIMOTO, H. KAWAKAMI, S. KATAYAMA: 'Elucidation of the effect of welding speed on melt flows in high-brightness and high-power laser welding of stainless steel on basis of three-dimensional X-ray transmission in situ observation', *Weld. Int.*, 31(3) (2017), 206-213.

[5] L. HUANG, X. HUA, D. WU, F. LI: 'Numerical study of keyhole instability and porosity formation mechanism in laser welding of aluminum alloy and steel', *J. Mater. Process. Technol.*, 252 (2018), 421-431.

[6] S. PANG, L. CHEN, J. ZHOU, Y. YIN, T. CHEN: 'A three-dimensional sharp interface model for self-consistent keyhole and weld pool dynamics in deep penetration laser welding', *J. Phys. D-Appl. Phys.*, 44 (2) (2011) 025301.

[7] H. WANG, M. NAKANISHI, Y. KAWAHITO: 'Dynamic balance of heat and mass in high power density laser welding', *Opt. Express*, 26 (5) (2018), 6392-6399.

[8] S. MUHAMMAD, S. W. HAN, S. J. NA, A. GUMENYUK, M. RETHMEIER: 'Numerical investigation of energy input characteristics for high-power fiber laser welding at different positions', *Int. J. Adv. Manuf. Tech.*, 80 (5) (2015), 931-946.

[9] Y. FENG, X. GAO, Y. ZHANG, C. PENG, X. GUI, Y. SUN, X. XIAO: 'Simulation and experiment for dynamics of laser welding keyhole and weld pool at different penetration status', *Int. J. Adv. Manuf. Tech.*, 112(7) (2021), 2301-2312.

[10] M. KERN, P. BERGER, H. HUEGEL, 'Magneto-fluid dynamic control of seam quality in CO2 laser beam welding', *Weld. J.*, 79 (3) (2000), 72-78.

[11] V. AVILOV, A. FRITZSCHE, M. BACHMANN, A. GUMENYUK, M. RETHMEIER: 'Full penetration laser beam welding of thick duplex steel plates with electromagnetic weld pool support', *J. Laser Appl.*, 28 (2) (2016) 022420.

[12] A. FRITZSCHE, K. HILGENBERG, F. TEICHMANN, H. PRIES, K. DILGER, M. RETHMEIER: 'Improved degassing in laser beam welding of aluminum die casting by an electromagnetic field', *J. Mater. Process. Technol.*, 253 (2018), 51-56.

[13] R. CHEN, C. WANG, P. JIANG, X. SHAO, Z. ZHAO, Z. GAO, C. YUE: 'Effect of axial magnetic field in the laser beam welding of stainless steel to aluminum alloy', *Mater. Des.*, 109 (2019), 146-152.

[14] M. GATZEN: 'Influence of low-frequency magnetic fields during laser beam welding of aluminium with filler wire', *Phys. Procedia*, 39 (2012), 59-66.

[15] X. MENG, M. BACHMANN, A. ARTINOV, M. RETHMEIER: 'Experimental and numerical assessment of weld pool behavior and final microstructure in wire feed laser beam welding with electromagnetic stirring', *J. Manu. Process*., 45 (2019), 408-418.

[16] M. BACHMANN, V. AVILOV, A. GUMENYUK, M. RETHMEIER: 'About the influence of a steady magnetic field on weld pool dynamics in partial penetration high power laser beam welding of thick aluminium parts', *Int. J. Heat Mass Transf.*, 60 (2013), 309-321.
[17] M. BACHMANN, V. AVILOV, A. GUMENYUK, M. RETHMEIER: 'Experimental and numerical investigation of an electromagnetic weld pool support system for high power laser beam welding of austenitic stainless steel', *J. Mater. Process. Technol.*, 214 (2014), 578-591.
[18] M. BACHMANN, V. AVILOV, A. GUMENYUK, M. RETHMEIER: 'Numerical simulation of full-penetration laser beam welding of thick aluminium plates with inductive support', *J. Phys. D-Appl. Phys.*, 45 (3) (2011) 035201.
[19] M. GATZEN, Z. TANG, F. VOLLERTSEN: 'Effect of electromagnetic stirring on the element distribution in laser beam welding of aluminium with filler wire', *Phys. Procedia*, 12 (2011) 56-65.
[20] R. ZHANG, X. TANG, L. XU, F. LU, H. CUI: 'Mechanism study of thermal fluid flow and weld root hump suppression in full penetration laser welding of Al alloy with alternating magnetic field support', *Int. J. Heat Mass Transf.*, 166 (2021) 120759.
[21] F. X. CHEN, M. LUO, R. HU, R. LI, L. LIANG, S. PANG: 'Thermo-electromagnetic effect on weld microstructure in magnetically assisted laser welding of austenite steel', *J. Manu. Process.*, 41 (2019), 111-118.
[22] X. MENG, A. ARTINOV, M. BACHMANN, M. RETHMEIER: 'Theoretical study of influence of electromagnetic stirring on transport phenomena in wire feed laser beam welding', *J. Laser Appl.*, 32 (2) (2020) 022026.
[23] X. MENG, A. ARTINOV, M. BACHMANN, M. RETHMEIER: 'Numerical and experimental investigation of thermo-fluid flow and element transport in electromagnetic stirring enhanced wire feed laser beam welding', *Int. J. Heat Mass Transf.*, 144 (2019) 118663.
[24] X. MENG, M. BACHMANN, A. ARTINOV, M. RETHMEIER: 'The influence of magnetic field orientation on metal mixing in electromagnetic stirring enhanced wire feed laser beam welding', *J. Mater. Process. Technol.*, 294 (2021) 117135.
[25] A. ARTINOV, N. BAKIR, M. BACHMANN, A. GUMENYUK, M. RETHMEIER: 'Weld pool shape observation in high power laser beam welding', *Procedia CIRP*, 74 (2018), 683-686.
[26] W. I. CHO, S. J. NA, C. THOMY, F. VOLLERTSEN: 'Numerical simulation of weld pool dynamics in high power disk laser welding', *J. Mater. Process. Technol.*, 212 (2012), 262-275.
[27] V. SEMAK, A. MATSUNAWA: 'The role of recoil pressure in energy balance during laser materials processing', *J. Phys. D-Appl. Phys.*, 30 (18) (1997) 2541.
[28] J. U. BRACKBILL, D. B. KOTHE, C. ZEMACH: 'A continuum method for modeling surface tension', *J. Comput. Phys.*, 100 (2) (1992), 335-354.
[29] Y. KAWAHITO, K. NAKADA, Y. UEMURA, M. MIZUTANI, K. NISHIMOTO, H. KAWAKAMI, S. KATAYAMA: 'Relationship between melt flows based on three-dimensional X-ray transmission in situ observation and spatter reduction by angle of incidence and defocussing distance in high-power laser welding of stainless steel', *Weld. Int.*, 32 (7) (2018), 485-496.
[30] D. ZHANG, M. WANG, C. SHU, Y. ZHANG, D. WU, Y. YE: 'Dynamic keyhole behavior and keyhole instability in high power fiber laser welding of stainless steel', *Opt. Laser Technol.*, 114 (2018), 1-9.
[31] R. LIN, H. P. WANG, F. LU, J. SOLOMON, B. E. CARLSON: 'Numerical study of keyhole dynamics and keyhole-induced porosity formation in remote laser welding of Al alloys', *Int. J. Heat Mass Transf.*, 108 (2017), 244-256.
[32] M. WU, A. VAKHRUSHEV, G. NUMMER, C. PFEILER, A. KHARICHA, A. LUDWIG: 'Importance of melt flow in solidifying mushy zone', *Open Transp. Phenom. J.*, 2 (2010), 16-23.
[33] P. F. MENDEZ: 'Characteristic values in the scaling of differential equations in engineering', *J. Appl. Mech.*, 77 (2010) 061017-1.

[34] W. TAN, Y. C. SHIN: 'Multi-scale modeling of solidification and microstructure development in laser keyhole welding process for austenitic stainless steel', *Comput. Mater. Sci.*, 98 (2015), 446-458.
[35] W. HUANG, H. WANG, T. RINKER, W. TAN: 'Investigation of metal mixing in laser keyhole welding of dissimilar metals', *Mater. Des.*, 195 (2020) 109056.
[36] L. J. ZHANG, J. X. ZHANG, A. GUMENYUK, M. RETHMEIER, S. J. NA: 'Numerical simulation of full penetration laser welding of thick steel plate with high power high brightness laser', *J. Mater. Process. Technol.*, 214 (8) (2014), 1710-1720.